Evolution of the phonon density of states of LaCoO_{3} over the spin state transition

N. O. Golosova, D. P. Kozlenko, A. I. Kolesnikov, V. Yu. Kazimirov, M. B. Smirnov, Z. Jirák, and B. N. Savenko

Evolution of the phonon density of states of LaCoO$_3$ over the spin state transition

N.O. Golosova[1], D.P. Kozlenko[1], A.I. Kolesnikov[2], V.Yu. Kazimirov[1], M.B. Smirnov[3], Z. Jirák[4], and B.N. Savenko[1]

[1] Frank Laboratory of Neutron Physics, Joint Institute for Nuclear Research, 141980 Dubna, Russia

[2] Neutron Scattering Sciences Division, Oak Ridge National Laboratory, Oak Ridge, TN 37831, USA

[3] Department of Physics, Saint-Petersburg State University, St-Petersburg, 194508, Russia

[4] Institute of Physics, Cukrovarnická 10, 162 53 Prague 6, Czech Republic

Abstract. The phonon spectra of LaCoO$_3$ were studied by inelastic neutron scattering in the temperature range of 4-120 K. The DFT calculations of the lattice dynamics have been made for interpretation of the experimental data. The observed and calculated phonon frequencies were found to be in a reasonable agreement. The evolution of the phonon density of states over the spin state transition was analyzed. In the low temperature range ($T < 50$ K) an increase of the energy of resolved breathing, stretching and bending phonon modes was found, followed by their softening and broadening at higher temperatures due to the spin state transition and relevant orbital-phonon coupling.

PACS: 63.20.-e, 63.20.dk, 75.30.Wx

I. INTRODUCTION

Among the transition metal oxides with perovskite-like structure the lanthanum cobaltite $LaCoO_3$ exhibits unusual electronic and magnetic properties.[1,2,3,4,5,6,7] At low temperature $LaCoO_3$ is a nonmagnetic semiconductor with a ground state of Co^{3+} ions of a low-spin (LS) configuration (t_{2g}^6, $S = 0$). The crystal field splitting energy of the ground state of the Co^{3+} ions in $LaCoO_3$ is comparable with the intra-atomic exchange energy[3,4], and a temperature driven spin state transition occurs due to gradual population of e_g electronic states, leading to formation of the paramagnetic state and sharp anomaly in the magnetic susceptibility at $T \sim 100$ K. In addition, a gradual semiconductor-metal transition accompanied by another broad anomaly in the magnetic susceptibility occurs in $LaCoO_3$ at $T \sim 500$ K.[4,6] Both susceptibility anomalies are also associated with the anomalies in the thermal lattice expansion.

The nature of the low temperature spin state transition in $LaCoO_3$ is still extensively debated. It is assumed that the thermally excited spin state can be either intermediate spin[4-7,8,9] (IS, $t_{2g}^5 e_g^1$) or high spin[10,11,12,13,14] (HS, $t_{2g}^4 e_g^2$) state, split by spin-orbital coupling. Recent infrared and Raman studies of $LaCoO_3$ have shown anomalous behavior of some optical phonon modes in the temperature range of the spin state transition.[15,16] It was attributed to the orbital phonon coupling, arising due to local lattice distortions, possibly associated with the Jahn-Teller effect, expected for the IS spin state.

In optical spectroscopy experiments, only a limited number of phonon modes can be studied, allowed by selection rules. The inelastic neutron scattering (INS) experiments provide an advantage to explore a temperature behavior of a full phonon spectrum. Previous INS studies of $LaCoO_3$ were concentrated on the study of phonon and magnetic excitations having relatively low energies in the range $0 - 30$ meV.[17,18,19] A softening of the E_g O – rotational and La vibrational modes was observed in the temperature region of the spin state transition.[17] However, the temperature behavior of the high-energy optical phonon modes remains less explored. In this

work, the evolution of the phonon density of states of $LaCoO_3$ is studied by the INS method in the extended energy transfer range 0 – 100 meV.

II. EXPERIMENTAL DETAILS

The synthesis procedure of powder $LaCoO_3$ sample is described in Ref. 9. Its crystal structure was tested by X-ray and neutron powder diffraction methods, giving an evidence to a single phase rhombohedrally distorted perovskite structure with the space group $R\overline{3}c$. The magnetic susceptibility, measured on a SQUID magnetometer using a DC field 100 Oe in the temperature range 4-300 K and corrected for the paramagnetic impurity contribution and diamagnetic contribution from the core electrons, is shown in fig. 1. It exhibits a maximum at $T \sim 100$ K, associated with the thermally induced spin state transition of Co^{3+} ions from the non magnetic ground state to the excited magnetic state, in accordance with previous studies. [3,6-8]

The inelastic neutron scattering experiments were performed on the High-Resolution Medium-Energy Chopper Spectrometer (HRMECS) at Intense Pulsed Neutron Source (IPNS), Argonne National Laboratory. A polycrystalline sample of 20 g was placed inside a sealed aluminum container. The INS data were taken with incident neutron energies E_0 = 35 and 110 meV over a wide range of scattering angles (28° - 140°) for a large coverage of momentum transfers. The measurements were performed at temperatures T = 4, 50, 75 and 120 K in the neutron energy loss mode. The energy resolution $\Delta E/E_0$ of the HRMECS spectrometer varied between 2 and 4%. Background scattering was subtracted from the data using an empty-container run. Detector calibration and intensity normalization were provided through measurements of elastic incoherent scattering from a vanadium standard. The experimental data were analyzed in the incoherent approximation[20,21], where the measured scattering function $S(Q,E)$ in the energy-loss mode is related to the generalized phonon density of states weighted by neutron scattering cross-section by

$$G^n(E) = B\left\langle \frac{e^{2W(Q)}}{Q^2} \frac{E}{n(E,T)+1} S(Q,E) \right\rangle$$

$$\approx C\sum_k \left\{ \frac{4\pi b_k^2}{m_k} \right\} g_k(E),$$

where the partial density of states $g_k(E)$ is given by

$$g_k(E) = D\int_{BZ} \sum_j \left| \xi(\mathbf{qj},k) \right|^2 \delta(E - E_j(q)) dq,$$

$$n(E, T) = [\exp(E/k_B T)-1]^{-1},$$

B, C and D are normalization constants, b_k and m_k are neutron scattering length and mass of kth atom, $E_j(q)$ and $\xi(\mathbf{qj},k)$ correspond to the energy and eigenvector of the jth phonon mode at wave vector q in the Brillouin zone (BZ). The symbol $\langle\ \rangle$ represents Q averaging of the quantities within. The data were properly averaged over the range of scattering angles to obtain the neutron-weighted generalized phonon density of states $G^n(E)$.

III. LATTICE DYNAMICS CALCULATIONS

According to group-theoretical analysis the following optical phonon modes are active for the Γ point of the Brillouin zone in the rhombohedrally distorted $LaCoO_3$ of $R\bar{3}c$ symmetry:

$$\Gamma = A_{1g} + 3A_{2g} + 4E_g + 2A_{1u} + 3A_{2u} + 5E_u,$$

five of which ($A_{1g}+4E_g$) are Raman active modes and eight of them ($3A_{2u} +5E_u$) are infrared (IR) active modes. [22] $3A_{2g}$ and $2A_{1u}$ modes are silent and not visible in optical spectroscopy experiments. La atoms participate in four Γ-point (zone center) phonon modes ($A_{2g}+A_{2u}+E_g+E_u$). While Co atoms contribute to four ($A_{1u}+A_{2u}+2E_u$) Γ-point phonon modes, O atoms take part in remaining ten Γ-point phonon modes in the rhombohedral lattice.

Density functional theory[23,24,25] (DFT) was applied to simulate the optimized atomic structure and lattice dynamics of $LaCoO_3$. The program $DMol^3$ was used for the *ab initio* calculations. In comparison with other prevalent DFT programs, the all-electron $DMol^3$ method[26,27] uses basis sets based on atomic orbitals and not on plane waves. This approach

provides an accurate treatment of interactions between core and valence shell electrons. The method incorporates fast convergent three-dimensional numerical integrations for a calculation of the matrix elements occurring in the Ritz variational method. The initial atomic configuration was taken from crystallographic data.[9] We employed the revised Perdew–Burke–Enserhof (RPBE) exchange-correlation functional[28,29] in generalized gradient approximation. The double numerical with polarization (DNP) atomic basis set with a real space cutoff of 9 bohr was used to ensure high accuracy of computations. The Monkhorst–Pack grid of $7 \times 7 \times 6$ points in k-space was used for Brillouin zone sampling. The calculated frequencies (Table I) are comparable with the available IR[15,30], Raman[16,31], and low energy INS[17] data.

IV. INS EXPERIMENTS

The INS spectrum measured at $E_0 = 35$ meV and $T = 4$ K is shown in Fig. 2. Three broad peaks are observed at 10, 14.2 and 16.7 meV. Following the previous INS and Raman studies[16,17], as well as the present DFT calculations (Table I), they are assigned to acoustic phonons (TA+LA), E_g rotational mode of O atoms and A_{2g} vibrational mode of La atoms, respectively.

Fig. 3 shows INS spectra taken at $E_0 = 110$ meV at different temperatures. In the energy transfer range 6-20 meV, they look similar to the data obtained at $E_0 = 35$ meV. In the energy transfer range 20 – 48 meV there is a broad intensity distribution with maxima located at around 25, 31.5, 36, 39 and 44 meV. According to previous studies[16,17] and our DFT calculations, the maxima correspond to E_g mode related to vibrations of La atoms (25.3 meV), A_{2u} mode related to bond bending vibrations of O and Co atoms (31.5 meV), A_{1g} mode related to rotations of O atoms around c-axis (35.6 meV), combination of E_u and A_{2g} (39.5 meV) and A_{1u} (44 meV) modes related to bond bending vibrations of O and Co atoms.

At the high-energy transfer range 48 – 90 meV, the INS spectra contain five distinctive peaks at around 52, 60, 68, 72 and 82 meV (fig. 3). Taking into account

previous results[15-17] and our calculations (Table I), these high energy peaks are associated with a combination of A_{2u}/E_u (52 meV) and E_g (60.5 meV) bending modes, combination of A_{2u}/E_u symmetric stretching modes (68.5 meV) related to Co and O atoms vibrations, E_g antisymmetric stretching mode (72 meV), and A_{2g} breathing mode (82.5 meV) related to oxygen vibrations.

The temperature dependences of the energies of the well-resolved optical phonon modes, obtained from INS spectra in the energy transfer range $48 - 90$ meV, are shown in fig. 4. They exhibit a weak increase at low temperature $T < 50$ K, and subsequent softening at higher temperatures due to a spin state transition, more pronounced for A_{2g} breathing and E_g bending modes and less pronounced for the E_g antisymmetric and A_{2u}/E_u symmetric stretching modes. Somewhat similar softening of the phonon modes was also found in Raman experiments.[16] It is associated with the anomalous contribution to thermal expansion of the Co-O bonds, caused by the gradual excitation of electrons from t_{2g} to e_g energy levels of Co^{3+} ions.[3,6-9]

The peaks corresponding to the E_g antisymmetric and A_{2u}/E_u symmetric stretching modes exhibit sharp broadening at $T \sim 60$-80 K, related to rapidly increasing population of the excited spin state, while broadening of the E_g, A_{2u}/E_u bending and A_{2g} breathing modes show more gradual character with a temperature increase (fig. 5).

Let us note that previous IR and Raman studies showed a splitting of optical phonon modes at the spin state transition.[15,16] This was attributed to local structure distortions, associated with the presence of the three different types of the Co-O bonds, Co(LS)-O-Co(LS), Co(LS)-O-Co(IS or HS), Co(IS or HS)-O-Co(IS or HS), which affected the phonon energies. The relevant redistribution of the phonon density of states can explain the additional broadening of the stretching phonon modes observed in the present INS experiment.

V. DISCUSSION

The peaks in INS spectra (figs. 2, 3) correspond to average phonon frequencies, weighted over the dispersion curves throughout the Brillouin zone. On the other hand, the frequencies determined by optical spectroscopy refer to Raman and IR active phonons at Brillouin zone center. Nevertheless, due to relatively flat dispersion curves of optical phonons[32], the positions of the observed peaks in INS spectra are well comparable to Raman and IR data of previous studies[15-17] – see Table I. They also show a similar temperature evolution with the course of the spin state transition. The observed softening and broadening of the optical breathing, stretching and bending phonon modes are related to the orbital-phonon coupling. It occurs due to gradual thermal population of the e_g orbitals of the Co^{3+} ions, causing local lattice distortions and affecting the interatomic distances and relevant force constants.

In previous Raman and IR studies[15,16] a special attention was given to the analysis of the intensity of particular phonon modes, which intensity correlates with the population of the ground or excited spin states due to sensitivity to local distortions. At the same time, a role of the spin state transition in the softening of the phonon modes frequencies has not been analyzed in detail.

The intensities of high energy optical phonon peaks observed in the INS data do not exhibit a noticeable variation in the temperature region of the spin state transition. This happens since they represent the bulk averaged phonon frequencies, weighted over the dispersion curves. The energies (frequencies) of bending and stretching modes depend on force constants, mediated by structural parameters. For the simplest case of the stretching modes, the phonon energy is related to distance between transition metal and oxygen atoms as $E \sim l^{-3/2}$.[33,34] The thermal expansion of the Co-O distance in $LaCoO_3$ at relatively low temperatures ($T < 150$ K) is dominated by the anomalous contribution due to the spin state transition[7] and it can be evaluated as $l/l_0 = x_0+(l_1/l_0)x_1$.[9] Here $l_{0,1}-$ equilibrium Co-O distances and $x_{0,1}=v_{0,1}\exp(-E_{0,1}/k_BT)/[1+v_1\exp(-E_1/k_BT)]$ – populations, corresponding to low spin and excited

spin states, respectively. The parameters $v_{0,1}$ are the degeneracy factors for ground and excited spin states ($v_0 = 1$ and $v_1 = 3$, Refs. 8, 9), $E_0 = 0$, and E_1 is the energy splitting between ground and excited spin states. The values $E_1 = 200$ K and $l_1/l_0 = 1.0072$ were calculated from fitting of temperature dependence of the average E_g antisymmetric stretching mode frequency, obtained from present INS data (Fig. 6). The obtained energy splitting value E_1 is comparable with previous estimations.[3, 5-10] From the values of ionic radii for Co^{3+} ion in different spin states, r_{LS} = 0.545, r_{IS} = 0.56 and r_{HS} = 0.61 Å, and known Co-O distance for low spin state $l_0 = 1.925$ Å (Ref. 7), one can evaluate ratio $l_1/l_0 = 1.0078$ for Co^{3+} in IS state and $l_1/l_0 = 1.0343$ for Co^{3+} in HS state. The first value is comparable with one obtained from the fitting of temperature dependence of the E_g antisymmetric stretching mode.

At the lowest temperature, the observed average frequency is notably smaller than extrapolation of the fit. There is evidently an additional structural reason for the drop of the E_g antisymmetric stretching mode energy in the low temperature region. An analysis of the structural data[7] of $LaCoO_3$ (fig. 6, inset) have shown that Co-O distance exhibits some decrease on temperature increase for $T < 50$ K, followed by increase at higher temperatures. Such changes in structural parameters may explain qualitatively the observed increase of this mode energy. It is worth mentioning that a decrease of the frequency of the E_g antisymmetric stretching mode below 50 K was also observed in Raman study.[35]

The dependence of bending modes frequencies on structural parameters is more complicated for a straightforward analysis, since one has to consider both bond stretching and angle bending force constants.[33] However, structural studies[7,9] have shown that spin state transition in $LaCoO_3$ affects mostly thermal evolution of Co-O and La-O bond lengths, while relevant changes of bond angles are much less pronounced. Therefore, the observed temperature behavior of the bending modes can be explained qualitatively by a change in bond stretching force constants, related to thermal evolution of Co-O and La-O distances.

CONCLUSIONS

In the present paper, the phonon spectrum of $LaCoO_3$ has been studied by a combination of INS experiments and theoretical DFT calculations. The predicted phonon frequencies are consistent with the experimentally resolved phonon peaks and their differences are less than 15%. The energies of resolved breathing, stretching and bending phonon modes increase at low temperature $T < 50$ K due to the peculiar behavior of structural parameters. At higher temperatures the spin state transition affects the phonon density of states by softening and additional broadening of these modes due to orbital-phonon coupling. The observed softening of the stretching and bending modes follows the anomalous thermal expansion of interatomic distances, caused by the spin state transition.

Table 1. Optical phonon modes for rhombohedral LaCoO$_3$: modes symmetry and frequencies. The experimental INS, Raman and infrared frequencies from present experiment and literature are also listed for comparison.

Mode	Frequency, calc. (DFT)		Activity	Experiment	
	cm^{-1}	meV		cm^{-1}	meV
E$_g$	82.0	10.2	Raman	114	14.2
				86[a]	10.7[a]
				104.8[b]	13.0[b]
A$_{2g}$	140.5	17.4	silent	135	16.7
				153[a]	18.9[a]
A$_{2u}$	166.6	20.7	IR	177.4[d]	22.0[d]
E$_g$	175.3	21.7	Raman	204	25.3
				172[a]	21.3[a]
				177.4[b]	22.0[b]
				162[c]	20.0[c]
E$_u$	185.5	23.0	IR	177.4[d]	22.0[d]
E$_u$	222.5	27.6	IR	242[d]	30.0[d]
A$_{1u}$	262.2	32.5	silent	254	31.5
A$_{1g}$	279.6	34.7	Raman	287	35.6
				261[a]	32.4[a]
E$_u$	331.9	41.2	IR	319	39.5 (E$_u$+A$_{2g}$)
				314.5[d]	39.0[d]
A$_{2g}$	335.9	41.7	silent	319	39.5 (E$_u$+A$_{2g}$)
				367[a]	45.5[a]
A$_{1u}$	358.8	44.5	silent	355	44.0
A$_{2u}$	419.6	52.0	IR	419	52.0 (A$_{2u}$+E$_u$)
E$_u$	425.6	52.8	IR	419	52.0 (A$_{2u}$+E$_u$)
				411.3[d]	51.0[d]
E$_g$	437.0	54.2	Raman	488	60.5
				432[a]	53.6[a]
				448[c]	55.6[c]
A$_{2u}$	531.8	65.9	IR	552	68.5 (A$_{2u}$+E$_u$)
				540[d]	67.0[d]
E$_u$	549.1	68.1	IR	552	68.5 (A$_{2u}$+E$_u$)
				540[d]	67.0[d]
E$_g$	600.0	74.4	Raman	581	72.0
				583[a]	72.4[a]
A$_{2g}$	700.7	86.9	silent	665	82.5
				677[a]	83.9[a]

a) Ref. 16
b) Ref. 17
c) Ref. 31
d) Ref. 15

Figure captions

Fig. 1. The magnetic susceptibility of $LaCoO_3$, corrected for the paramagnetic impurity contribution and diamagnetic contribution from the core electrons.

**Fig. 2.** The INS spectrum of $LaCoO_3$ taken at $E_0 = 35$ meV and $T = 4$ K.

Fig. 3. The INS spectra of $LaCoO_3$ taken at $E_0 = 110$ meV at different temperatures. The ticks below represent the phonon modes frequencies calculated by DFT (Table I). Solid line represents the interpolation by a set of Gaussian functions, which positions were initially fixed to the calculated phonon modes (Table I) and refined subsequently. For the high-energy phonons, a contribution from individual Gaussian functions is also shown by dashed lines.

Fig. 4. Temperature dependences of the high-energy optical phonon frequencies obtained from INS data. Lines are guides for eyes only.

Fig. 5. Temperature dependencies of the full width at half maximum of the INS peaks corresponding to breathing, stretching and bending optical phonon modes. Lines are guides for eyes only.
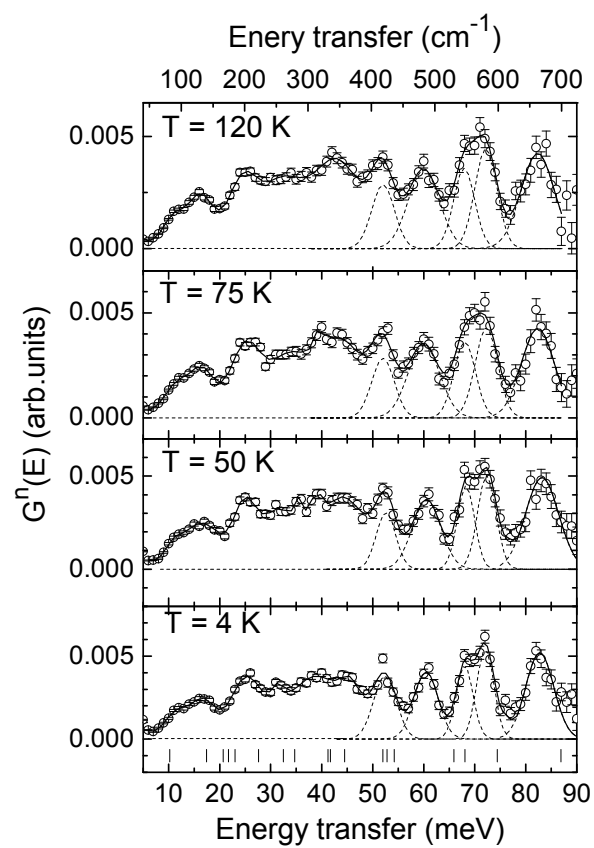
Fig. 6. The temperature dependencies of E_g antisymmetric stretching mode and Co-O bond length (inset, data taken from Ref. 7), interpolated as described in the text.
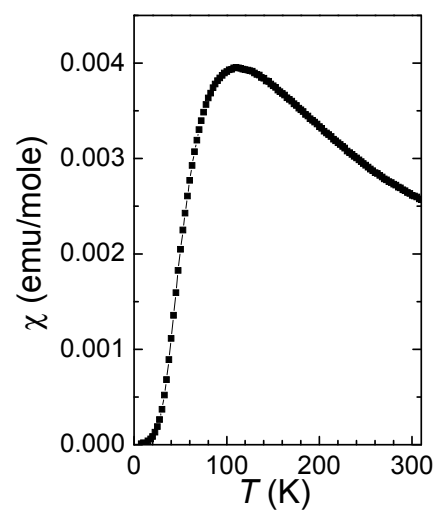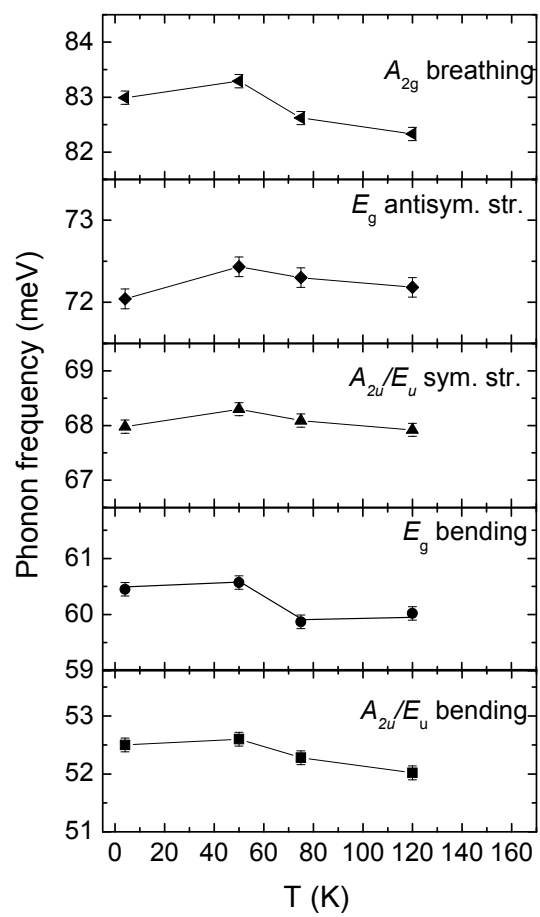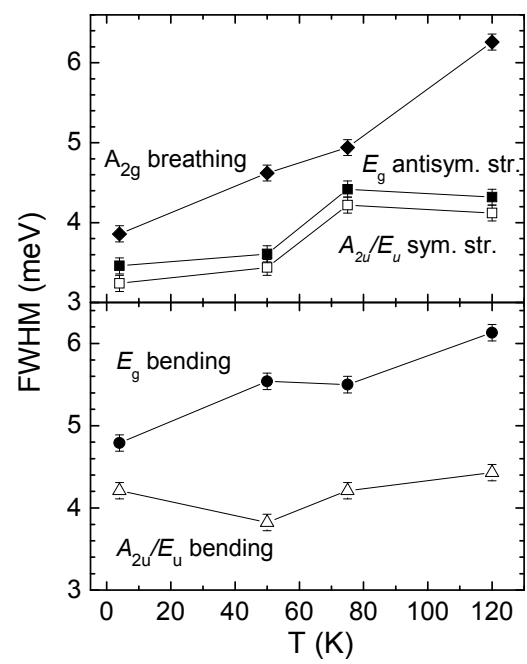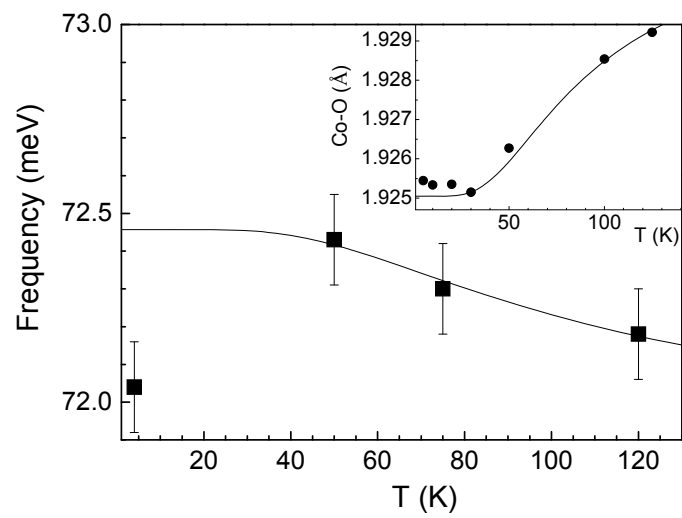
Fig. 1.
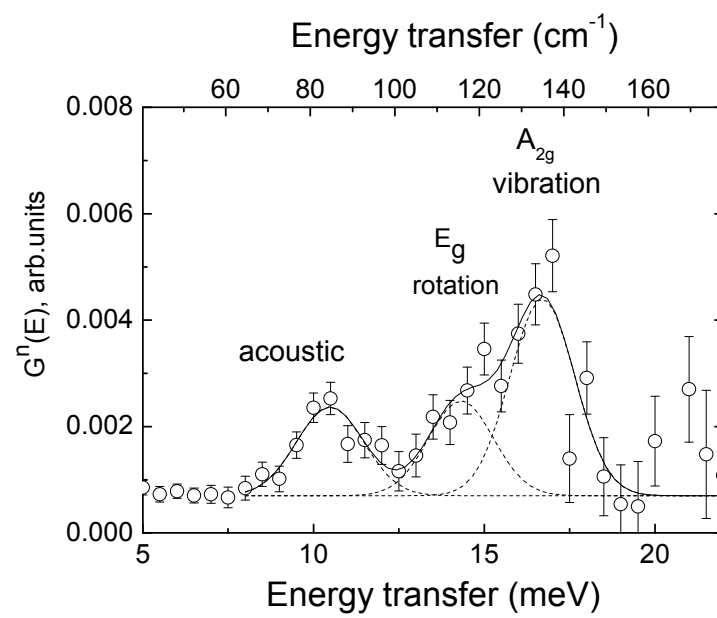
Fig. 2.

Fig. 3.

Fig. 4.

Fig. 5.

Fig. 6.

[1] R. R. Heikes, R. C. Miller, and R. Mazelsky, Physica **30**, 1600 (1964).

[2] P. M. Raccah and J. B. Goodenough, Phys. Rev. **155**, 932 (1967).

[3] M. A. Señarís-Rodríguez and J. B. Goodenough, J. Solid State Chem. **116**, 224 (1995).

[4] R. Potze, G. A. Sawatzky, and M. Abbate, Phys. Rev. B **51**, 11501 (1995).

[5] M. A. Korotin, S. Yu. Ezhov, I. V. Solovyev, V. I. Anisimov, D. I. Khomskii, and G. A. Sawatzky, Phys. Rev. B **54**, 5309 (1996).

[6] K. Asai, A. Yoneda, O. Yokokura, J. M. Tranquada, G. Shirane, and K. Kohn, J. Phys. Soc. Jpn **67**, 290 (1998).

[7] P. G. Radaelli and S.-W. Cheong, Phys. Rev. B **66**, 094408 (2002).

[8] C. Zobel, M. Kriener, D. Bruns, J. Baier, M. Grüninger, T. Lorenz, P. Reutler, and A. Revcolevschi, Phys. Rev. B **66**, 020402 (2002).

[9] D.P.Kozlenko, N.O.Golosova, Z.Jirák, L.S.Dubrovinsky, B.N.Savenko, M.G.Tucker, Y. Le Godec, and V.P.Glazkov, Phys. Rev. B **75**, 064422 (2007).

[10] S. Noguchi, S. Kawamata, K. Okuda, H. Nojiri, and M. Motokawa, Phys. Rev. B **66**, 094404 (2002).

[11] Z. Ropka and R.J. Radwanski, , Phys. Rev. B 6**7**, 172401 (2003).

[12] M.W.Haverkort, Z. Hu, J.C. Cezar, T. Burnus, H. Hartmann, M. Reuther, C. Zobel, T. Lorenz, A. Tanaka, N.B. Brookes, H.H. Hsieh, H.-J. Lin, C.T. Chen, and L.H. Tjeng, Phys. Rev. Lett. **97**, 176405 (2006).

[13] T.Kyômen, Y. Asaka, M. Itoh, Phys. Rev. B **71**, 124418 (2005).

[14] M.J.R.Hoch, S. Nellutla, J. van Tol, E.S. Choi, J. Lu, H. Zheng, and J.F. Mitchell, Phys. Rev. B **79**, 214421 (2009).

[15] S. Yamaguchi, Y. Okimoto, and Y. Tokura, Phys. Rev. B **55**, R8666 (1996).

[16] A. Ishikawa, J. Nohara, and S. Sugai, Phys. Rev. Lett. **93**, 136401 (2004).

[17] Y. Kobayashi, T. S. Naing, M. Suzuki, M. Akimitsu, K. Asai, K. Yamada, J. Akimitsu, P. Manuel, J. M. Tranquada, and G. Shirane, Phys. Rev. B **72**, 174405 (2005).

[18] D. Louca and J. L. Sarrao, Phys. Rev. Lett. **91**, 155501 (2003).

[19] A.Podlesnyak, S. Streule, J. Mesot, M. Medarde, E. Pomjakushina, K. Conder, A. Tanaka, M.W. Haverkort, and D.I. Khomski, Phys. Rev. Lett. **97**, 247208 (2006).

[20] D.L. Price and K. Skold, in *Neutron Scattering*, ed. by K. Skold and D.L. Price, (Academic Press, Orlando, 1986), vol. A.

[21] J.M. Carpenter and D.L. Price, Phys. Rev. Lett. **54**, 441 (1985).

[22] M.V. Abrashev, A.P. Litvinchuk, M.N. Iliev, R.L. Meng, V.N. Popov, V.G. Ivanov, R.A.Chakalov, and C. Thomsen, Phys. Rev. B **59**, 4146 (1999).

[23] R.G. Parr, W. Yang, *Density-Functional Theory of Atoms and Molecules*, (Oxford University Press, New York, 1989).

[24] R. Dreizler, E. Gross, *Density Functional Theory*, (Plenum Press, New York, 1995).

[25] W. Koch and M.C. Holthausen, *A Chemist's Guide to Density Functional Theory*, (Wiley-VCH, Weinheim, ed. 2, 2002).

[26] B. Delley, J. Chem. Phys. **92**, 508 (1990).

[27] B. Delley, J. Chem. Phys. 113 (18) (2000) 7756.

[28] J.P. Perdew, K. Burke, M. Ernzerhof, Phys. Rev. Lett. **77**, 3865 (1996).

[29] B. Hammer, L.B. Hansen, J.K. Norskov, Phys. Rev. B **59**, 7413 (1999).

[30] S. Tajima, A. Masaki, S. Uchida, T. Matsuura, K. Fueki, and S. Sugai, J. Phys. C: Solid State Phys. **20**, 3469 (1986).

[31] N. Orlovskaya, D. Steinmetz, S. Yarmolenko, D. Pai, J. Sankar, and J. Goodenough, Phys. Rev. B **72**, 014122 (2005).

[32] D. Reznik and W. Reichardt, Phys. Rev. B **71**, 092301 (2005).

[33] A. de Andrés, S. Taboada, J.L. Martínez, A. Salinas, J. Hernández, and R. Sáez-Puche, Phys. Rev. B **47**, 14898 (1993).

[34] L. Martín-Carrón, A. de Andrés, M. J. Martínez-Lope, M. T. Casais, and J. A. Alonso, Phys. Rev. B **66**, 174303 (2002).

[35] Md.M. Seikh, L. Sudheendra, C. Narayana, C.N.R.Rao, J. Mol. Str. 706, 121 (2004).